Available online at www.sciencedirect.com
ScienceDirect
Ceramics International 36 (2010) 2337–2344
CERAMICS INTERNATIONAL
www.elsevier.com/locate/ceramint

Relationship between fracture toughness characteristics and morphology of sintered Al_2O_3 ceramics

Kuntal Maiti, Anjan Sil *

Department of Metallurgical and Materials Engineering, Indian Institute of Technology Roorkee, Roorkee 247 667, Uttarakhand, India

Received 13 January 2010; received in revised form 12 April 2010; accepted 7 June 2010
Available online 3 August 2010

Abstract

The influence of sintering temperature and soaking time on fracture toughness of Al_2O_3 ceramics has been investigated. The samples were prepared by solid state sintering at 1500, 1600 and 1700 °C for different soaking time periods. The fracture toughness of the sintered samples was determined by inducing cracks using Vickers indentation technique. Microstructural investigations on fracture surfaces obtained by three point bend test mode were made and correlated with fracture toughness. Crack deflection in the samples sintered at 1500 and 1600 °C for which ranges of fracture toughness are 5.2–5.4 and 5.0–5.6 MPa $m^{1/2}$ respectively, are found. The samples sintered at 1700 °C have lower fracture toughness ranging between 4.6 and 5.0 MPa $m^{1/2}$. These samples have larger grains and transgranular fracture mode is predominant. The crack deflection has further been revealed by SEM and AFM observations on fracture surface and fracture surface roughness respectively.

Keywords: A. Sintering; C. Hardness; D. Al_2O_3; Fracture toughness

1. Introduction

Dense Al_2O_3 is a widely used ceramic material because of its high hardness, good wear resistance and outstanding mechanical properties at room temperature as well as at higher temperatures. But low flexural strength and low fracture toughness, limit this material from being used as cutting tool, cylinder liner, valve seat, piston ring in automotive engine and mechanical seal. Deng et al. [1] reported that the increase in fracture toughness of Al_2O_3/SiC composite is due to the change in fracture mode from transgranular in dopant-free composites to intergranular in rare earth (RE) doped composites. Jang et al. [2] reported the improvement in mechanical properties of Al_2O_3 ceramics by using Al_2O_3/SiC composites. West et al. [3] reported the effect of the RE grain boundary segregation on mode of fracture in Al_2O_3. The RE doping results in an increased proportion of intergranular fracture relative to the undoped material having similar grain size. This is due to the RE dopant, which segregates to grain boundaries reducing grain boundary cohesion [4]. Chow and Tuan [5] reported the fracture toughness enhancement of Al_2O_3 by making Al_2O_3/Ag composites, due to the crack deflection and crack bridging mechanisms. The mechanical properties especially wear behaviour of Al_2O_3/SiC ceramic composites and the mechanism of fracture have been discussed by Zhang et al. [6]. The influence of grain size and grain morphology on strength variability in Al_2O_3 ceramics was demonstrated by Kovar et al. [7]. The Al_2O_3 ceramic shows good R-curve behaviour which may be due to grain bridging effect and this toughening mechanism along with grain pullout has been widely reported in silicon nitride ceramics and whiskers reinforced ceramics [8,9]. However, issues on toughening mechanisms for pure oxide ceramics have, to the best of the authors' knowledge, not been fully settled as to which one plays a crucial role in the toughness enhancement. To address such issue microstructural dependence has been considered as primarily important. The purpose of the present work is to establish a link between the ceramic microstructure that develops on sintering without any additive and the resulting fracture toughness of the material prepared. To fulfill the objective, Al_2O_3 ceramics were prepared by solid state sintering process at three different temperatures of 1500, 1600 and 1700 °C for different soaking time periods with an idea to generate varied grain size and grain shape. The

* Corresponding author. Tel.: +91 1332 285073; fax: +91 1332 285243/273560.
E-mail address: anj_sil@yahoo.co.uk (A. Sil).

0272-8842/$36.00
doi:10.1016/j.ceramint.2010.07.031

microstructures of single phase ceramic materials generally consist of non-uniform grains. The effect of different dopants on the sintering behaviour of Al_2O_3 has been explained by Park [10]. The grain morphology is controlled by the chemical reaction of dopants used with Al_2O_3 ceramic producing liquid phase during sintering. However, in the present study an attempt has been made to develop the variability in grain morphology by solid state sintering of pure Al_2O_3 ceramics without using any additive. In general microstructural and morphological features play leading roles in the emergence of properties of ceramic materials. For monolithic Al_2O_3, only coarse grains, elongated grains and grains with high aspect ratio, can result in an increase in fracture toughness. Such improvement can be attributed to the mechanisms of crack bridging and crack deflection [11,12]. Tani et al. [13] reported that fracture toughness of Al_2O_3 ceramics decreases sharply with increasing grain size. Further fracture toughness can alternatively be viewed through the measure of fracture surface roughness as intergranular mode of fracture leads to larger roughness compared to that for fracture by transgranular mode. In this context a correlation between fracture surface roughness and fracture toughness of Al_2O_3 platelets reinforced glass matrix composites has been reported [14].

2. Experimental procedure

The raw material used is Al_2O_3 powder (99.8%, 0.4 μm) which was mixed with required quantity of binder (polyvinyl alcohol) for granulation. The granulated powder was compacted in the form of rectangular bar having dimension 3 mm × 5 mm × 45 mm, uniaxially in a hydraulic press at different loads ranging between 15×10^4 and 22.5×10^4 N. The green compacts were sintered at 1500 °C for different soaking time periods of 3, 6, 9, 12, 18, 24 and 36 h. Samples were prepared also by sintering at 1600 and 1700 °C for the soaking time periods of 3, 6, 9 and 12 h. The rate of heating as well as cooling used in the sintering process was 10 °C/min. The density of all samples was measured following Archimedes principle using water as an immersion medium. However, the measured density data are presented in the text as relative densities by taking the theoretical density of the Al_2O_3 is 3.97 gm/cc. The samples were ground by silicon carbide (SiC) papers having mesh sizes of #120, #220, #320 to develop smooth surface finish on one face. The smooth surfaces of the samples were polished with diamond paste having two different grades of 6 and 3 μm sizes, to the level of near mirror finish, and indented by various loads of 5, 10, 15, 20, 30 and 40 kg for an identical dwell time of 15 s. The indentations were carried out at ambient conditions. The length of each diagonal of the square shaped Vickers indentation and crack length generated from the corners and boundaries of the indentation impression were measured by optical microscope (Axiovert 200 MAT, ZEISS). The hardness (H_v) of each sample was calculated from the equation given below:

$$H_v = \frac{P}{A} = \alpha \frac{P}{{d_o}^2} \quad (1)$$

where P is the applied load, A is the pyramidal contact area of the indentation, d_o is the average length of the diagonals of the resultant impression and $\alpha = 1.8544$ for Vickers indenter.

The resultant crack length for each indentation has been estimated by taking the average of all the crack lengths produced due to the indentation and hence the fracture toughness (K_{IC}) was determined following the relationship given below [15]:

$$K_{IC} = \chi \left(\frac{E}{H_v}\right)^{1/2} \frac{P}{c^{3/2}} \quad (2)$$

where E is Young's modulus; H_v, the Vickers hardness; c, the radial crack length measured from the centre of the indent and χ, an empirical calibration constant which has been taken as 0.016 ± 0.004.

Microstructural observations were made using FESEM (FEI, QUANTA 200F) to determine the grain structure of the sintered samples. The polished sample surface was gold coated for the microstructural observation. The grain size from the micrographs was calculated using Image J software. Roughness of the fracture surface was determined with the help of AFM (NT-MDT Integra).

3. Results and discussion

3.1. Microstructural analysis

The Al_2O_3 samples prepared by different sintering schedules are designated in the text by $A_{t(h)}^{T(°C)}$ (e.g. A_3^{1500} represents the pure Al_2O_3 sample sintered at 1500 °C and soaked for 3 h). Fig. 1(a)–(d) shows the SEM micrographs of Al_2O_3 samples sintered at 1500 °C for four different soaking time periods of 3, 6, 18 and 24 h. The micrographs in Fig. 1 show the increase in average grain size with the increase in soaking time period. The estimated grain size ranges are given in Table 1. As evident from the micrographs, the samples consist of grains having varied sizes. The grains in Fig. 1(a) are smaller and have almost rounded shape. It can be observed from Fig. 1(a) that at some regions the grains tend to join together to give rise to larger grains. The estimated grain size varies between 0.2 and 1.3 μm.

Fig. 1(b) shows that the average grain size is slightly bigger than that in Fig. 1(a). The grains are of mixed sizes. The smaller grains are of rounded shape and larger grains appear to be elongated. The range of grain size is 0.3–1.9 μm. In Fig. 1(c) and (d), the occurance of exaggarated grain growth is evident. The larger grains are seen to have been developed from a number of smaller grains joined preferentially by surface diffusion process. The larger grains are also seen surrounded by a number of smaller grains. As can be observed from Table 1, that exaggerated grain growth occurs in the samples when the sintering was done at 1500 °C for a soaking time period of 18 h or more. Therefore a large grain size difference is resulted in all the samples sintered at 1500 °C and soaking for 18, 24 and 36 h.

Fig. 2(a)–(c) shows the SEM micrographs of Al_2O_3 samples sintered at 1600 °C for the soaking time periods of 3, 9 and 12 h

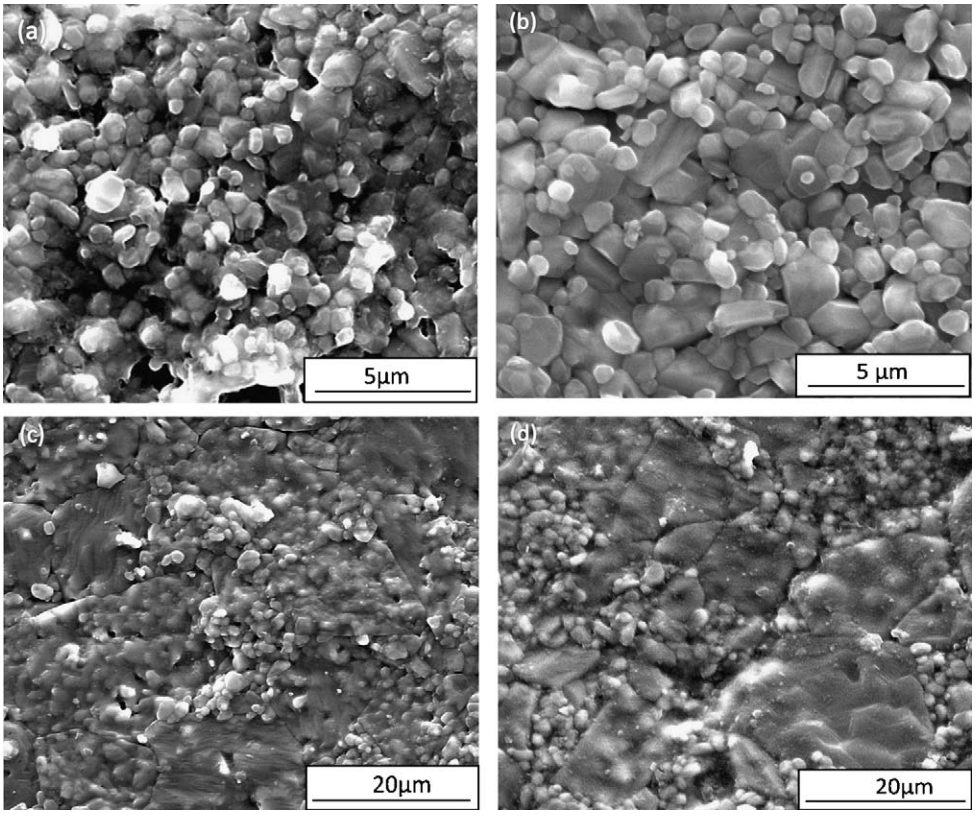

Fig. 1. SEM micrograph of Al_2O_3 sintered at 1500 °C for (a) 3 h, (b) 6 h, (c) 18 h and (d) 24 h.

respectively. The average grain size in this case is larger relative to the grains in the samples sintered at 1500 °C. The grain size range for these samples is also larger than that for the samples sintered at 1500 °C. It can be seen from Fig. 2 that the microstructure has sharp grain boundaries compared to those of the samples sintered at 1500 °C. Fig. 2(a) shows the combination of smaller and larger grains whose size varies between 1.5 and 21.4 μm. Fig. 2(b) shows the larger and smaller grains with a few larger grains having high aspect ratio and this microstructure is suitable to offer crack bridging as the possible mechanism of fracture toughness enhancement which has been discussed later. In Fig. 2(c) the grain size varies from 2.8 to 25.8 μm. However, in all these samples grain structures are very compact with less porosity.

Fig. 3(a) and (b) shows the SEM micrographs of Al_2O_3 samples sintered at 1700 °C for 3 and 12 h respectively. Fig. 3(a) shows that the grains are nearly equiaxed and polygonal type. The range of grain size is 3.0–26.4 μm. Fig. 3(b) shows that majority of the grains are larger and nearly equiaxed. The range of grain size is 4.3–41.2 μm.

Table 1
Grain size, relative density, hardness and fracture toughness of Al_2O_3 samples sintered at 1500, 1600 and 1700 °C.

Sample	Grain size range (μm)	Grain size difference (μm)	Relative density (%)	Hardness (GPa)	Fracture toughness (MPa $m^{1/2}$)
A_3^{1500}	0.2–1.3	1.1	96.7	13.0	5.2 ± 0.4
A_6^{1500}	0.3–1.9	1.6	98.0	12.7	5.2 ± 0.2
A_9^{1500}	0.4–2.0	1.6	98.5	12.4	5.4 ± 0.5
A_{12}^{1500}	0.4–2.0	1.6	98.5	13.2	5.4 ± 0.5
A_{18}^{1500}	1.0–16.9	15.9	98.7	11.0	5.3 ± 0.2
A_{24}^{1500}	1.3–17.6	16.3	98.7	9.2	5.3 ± 0.2
A_{36}^{1500}	1.3–19.6	18.2	98.7	4.1	5.3 ± 0.4
A_3^{1600}	1.5–21.4	19.9	98.5	6.6	5.4 ± 0.4
A_6^{1600}	2.2–21.8	19.6	98.5	6.1	5.5 ± 0.3
A_9^{1600}	2.7–22.6	19.9	98.5	6.4	5.6 ± 0.5
A_{12}^{1600}	2.8–25.8	23	98.7	7.2	5.0 ± 0.4
A_3^{1700}	3.0–26.4	23.4	98.5	6.7	4.6 ± 0.5
A_6^{1700}	3.3–33.5	30.2	98.7	7.1	5.0 ± 0.5
A_9^{1700}	3.7–40.9	37.2	99.0	7.2	4.9 ± 0.3
A_{12}^{1700}	4.3–41.2	36.9	98.7	6.0	5.0 ± 0.6

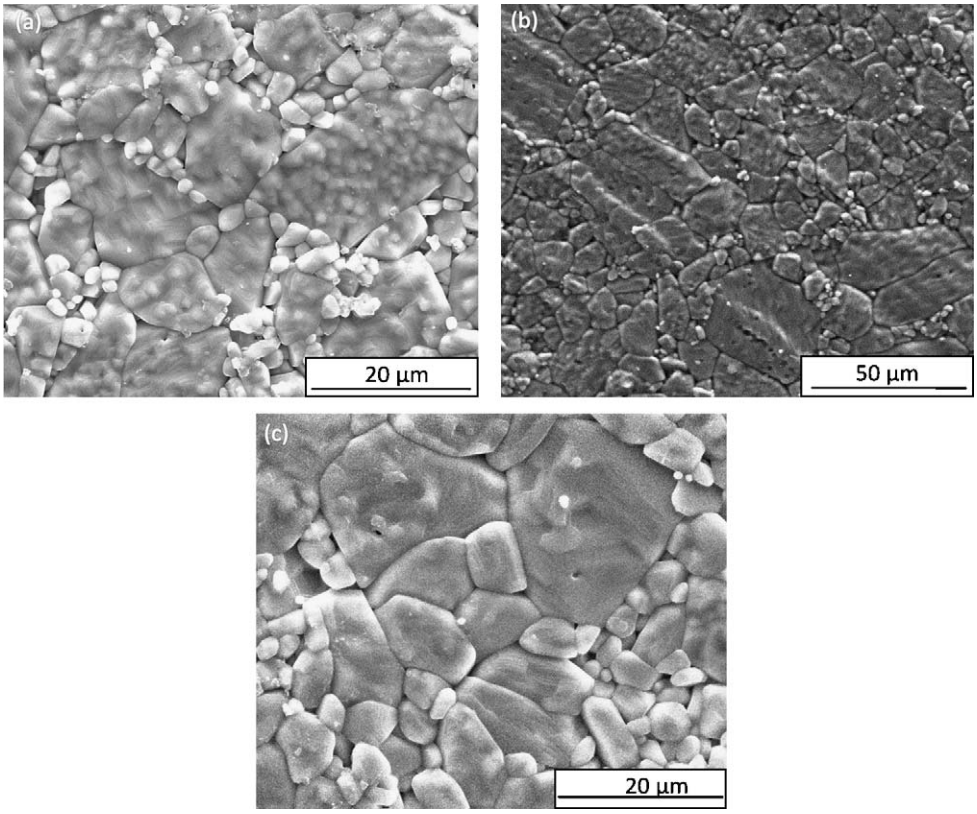

Fig. 2. SEM micrographs of Al_2O_3 sample sintered at 1600 °C for (a) 3 h, (b) 9 h and (c) 12 h.

3.2. Fracture toughness

Table 1 shows the relative density, grain size and mechanical properties i.e. hardness and fracture toughness of pure Al_2O_3 samples. Though the relative densities of the samples sintered at 1500 °C for 3 and 6 h are marginally lower, the uniform relative density of 98.5–99.0% has been achieved for all other samples sintered at all the three temperatures. Therefore the effect of the density variation on the resulting mechanical properties of the samples is not significant. Rice et al. reported, porosity of the samples increases with increasing grain size affecting the mechanical properties of the materials [16]. It is presumably the thermal stress that develops during cooling in the sintering process, results in the variation of the mechanical properties of the sintered samples. The internal stress in the samples having larger grains that develops during cooling, generates small cracks which affect the hardness as well as fracture toughness of the materials [17,18].

Hardness values of the samples sintered at 1500 °C for soaking up to 12 h are nearly same varying marginally from 12.4 to 13.2 GPa. The samples sintered at 1500 °C, however, for longer soaking times such as 18 and 24 h, show hardnesses of 11.0 and 9.2 GPa respectively. Therefore the majority of the samples sintered at 1500 °C show the hardness in the range of 13.2–9.2 GPa. The sample for which the soaking time was 36 h, results in lower hardness of 4.1 GPa. The lower hardness is attributed to the larger grain size developed due to higher soaking time period [19,20]. The hardness values of the samples sintered

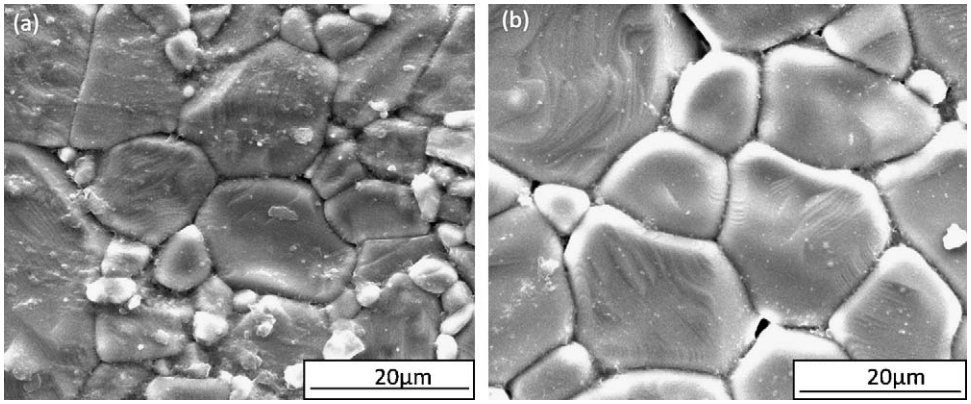

Fig. 3. SEM micrograph of Al_2O_3 sample sintered at 1700 °C for (a) 3 h and (b) 12 h.

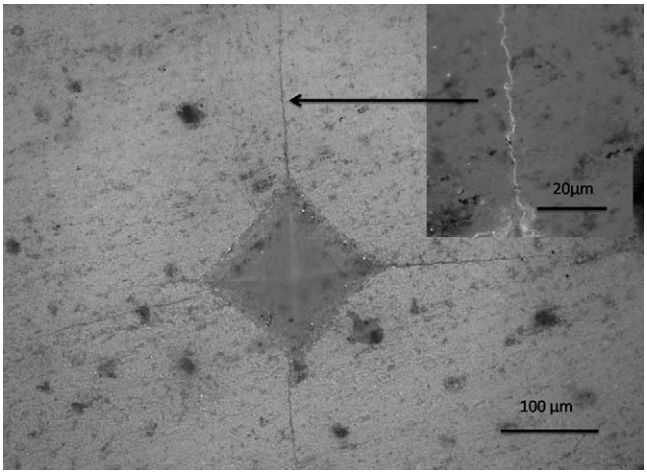

Fig. 4. Vickers's indentation with crack in the Al_2O_3 samples sintered 1600 °C for 3 h.

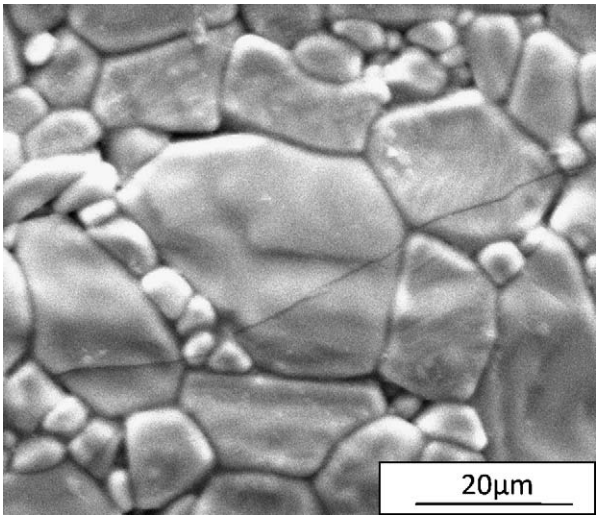

Fig. 6. SEM micrograph of Al_2O_3 sample sintered at 1700 °C for 3 h.

at 1600 and 1700 °C for the soaking times of 3, 6, 9 and 12 h studied are in the range of 6.0–7.2 GPa. Fig. 4 shows an optical micrograph of the Vickers indentation showing the cracks are emanating from the corners of the indentation in Al_2O_3 samples sintered at 1600 °C for 3 h. An enlarged view of one crack path is shown in an inset of Fig. 4. The zigzag nature of the crack path as can be seen in the inset indicates the crack propagation with associated crack deflection behaviour in the sample.

As a typical case, further enlargement of the partial crack path shown in Fig. 4 is presented in Fig. 5 to reveal the mode of crack propagation. Fig. 5 shows that the crack propagation is mainly intergranular in nature indicating the crack deflection is the predominant mechanism for higher toughness (5.4 ± 0.4 MPa $m^{1/2}$) resulted in this sample.

The micrograph in Fig. 6 shows that in the sample sintered at 1700 °C for 3 h, the crack propagation is transgranular. The transgranular fracture is the consequence to lower facture toughness of the samples sintered at 1700 °C for almost all the soaking time periods considered. Micrographs of Figs. 5 and 6 were taken after the indentation of the as sintered samples.

Fracture toughness of the samples sintered at 1500 °C varies from 5.2 ± 0.2 to 5.4 ± 0.5 MPa $m^{1/2}$ considering all the soaking time periods. The samples sintered at 1600 °C show marginally higher fracture toughness, the range of which is 5.0 ± 0.4–5.6 ± 0.5 MPa $m^{1/2}$. Fracture toughness of the samples sintered at 1700 °C is slightly lower than that obtained for the samples sintered at 1500 and 1600 °C and the value lies in the range of 4.6 ± 0.5–5.0 ± 0.6 MPa $m^{1/2}$.

The sintering process resulted in grain shape variation which has been taken into account by calculating aspect ratio (AR) parameter for several grains in the samples sintered at 1500, 1600 and 1700 °C for one particular soaking period of 9 h as an example and the calculated ARs are presented in Table 2. The ARs of the grains considering the samples sintered at all the three temperatures, are found to lie between 1.0 and 2.85. These values are further shown (in Table 2) subdivided into following three different ranges of (i) 1.0–1.30, (ii) 1.31–1.80 and (iii) 1.81–2.85 for each sample to indicate the degree of deviation of the grain shape from the regular equiaxed nature. The values in the same row correspond to a same range. Table 2 shows the grains having AR ranges of 1.0–1.30 and 1.31–1.80 are nearly comparable in number for the samples sintered at 1500, 1600 and 1700 °C. However, the grains having AR in the range of 1.81–2.85 are significantly more in number for the samples sintered at 1600 °C than the samples sintered at 1500 and

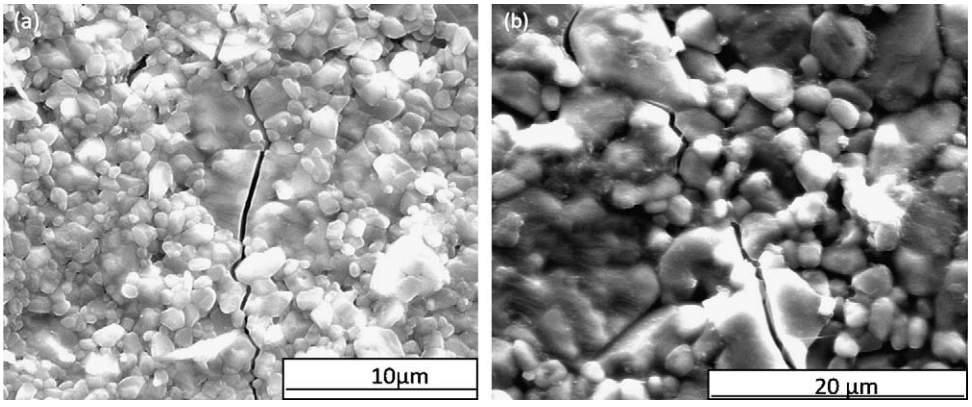

Fig. 5. SEM micrograph of Al_2O_3 sample sintered at (a)1500 °C for 3 h and (b) 1600 °C for 3 h.

Table 2
Aspect ratio (AR) of the samples sintered at 1500, 1600 and 1700 °C for the soaking time periods of 9 h.

AR of A_9^{1500} samples	AR of A_9^{1600} samples	AR of A_9^{1700} samples
1.01,1.05,1.09,1.11,1.13,1.15,1.15, 1.15,1.16,1.18,1.21,1.21,1.22,1.23, 1.24,1.25,1.29,1.29	1,1.02,1.02,1.08,1.11,1.19,1.19,1.23, 1.23,1.23,1.25,1.27,1.28,1.28	1.02,1.03,1.06,1.07,1.08, 1.09, 1.18,1.18,1.19,1.21, 1.21,1.23, 1.24,1.25,1.29
1.31,1.36,1.43,1.44,1.45,1.51, 1.51,1.51, 1.52,1.54,1.55,1.58, 1.67,1.69,1.72,1.73,1.79	1.32,1.38,1.38,1.43,1.43,1.47,1.48,1.51, 1.54,1.56,1.56,1.57,1.58,1.61,1.62,1.66,1.67	1.34,1.34,1.35,1.36,1.36,1.39, 1.41,1.44,1.46,1.48,1.48,1.51, 1.55,1.61,1.64,1.64,1.64,1.64
1.91,2.04,2.34	1.84,1.86,1.91,1.95,1.96,2.12, 2.18,2.23,2.5,2.74	1.85,2.02,2.28,2.85

1700 °C. Therefore the contribution of grain bridging effect towards the higher fracture toughness of the samples sintered at 1600 °C for a soaking time of 9 h is perhaps important [7].

3.3. Microstructures of the fracture surfaces

In order to relate the mode of crack propagation on the sample surface due to indentation, with the failure mode operative in the bulk of the sample, microstructures of the fracture surfaces of the samples were studied. Micrographs of the fracture surfaces of the samples sintered at 1500, 1600 and 1700 °C are shown in Fig. 7. The fracture surfaces were generated from these samples which were subjected to three point bend test. In Fig. 7(a) the presence of smaller grains is clear and the surface topography shows that the fracture has taken place predominantly due to the intergranular mode. It is more clear from Fig. 7(b) that the smaller grains remain in almost the same size range as obtained in the case of Fig. 7(a), however the larger grains have grown substantially in relation to that in Fig. 7(a). This observation matches well with the microstructure of the sample surface as given in Fig. 1(c). Further the fracture surface morphology confirms that the fracture has taken place due to mixed mode of intergranular and transgranular fracture, with larger proportion of the intergranular mode. The fracture toughnesses of these samples (Fig. 7(b) and (c)) show relatively higher toughness as listed in Table 1. But in Fig. 7(d) the flat fracture surface morphology over a considerable region in the micrograph area shows that the fracture has occurred predominantly due to the transgranular mode. The lower fracture toughness obtained is the obvious consequence to such fracture surface feature [21]. Fig. 7(c) shows that a large portion of grain structure area is occupied by large grains with smaller area portion filled with smaller sized grains.

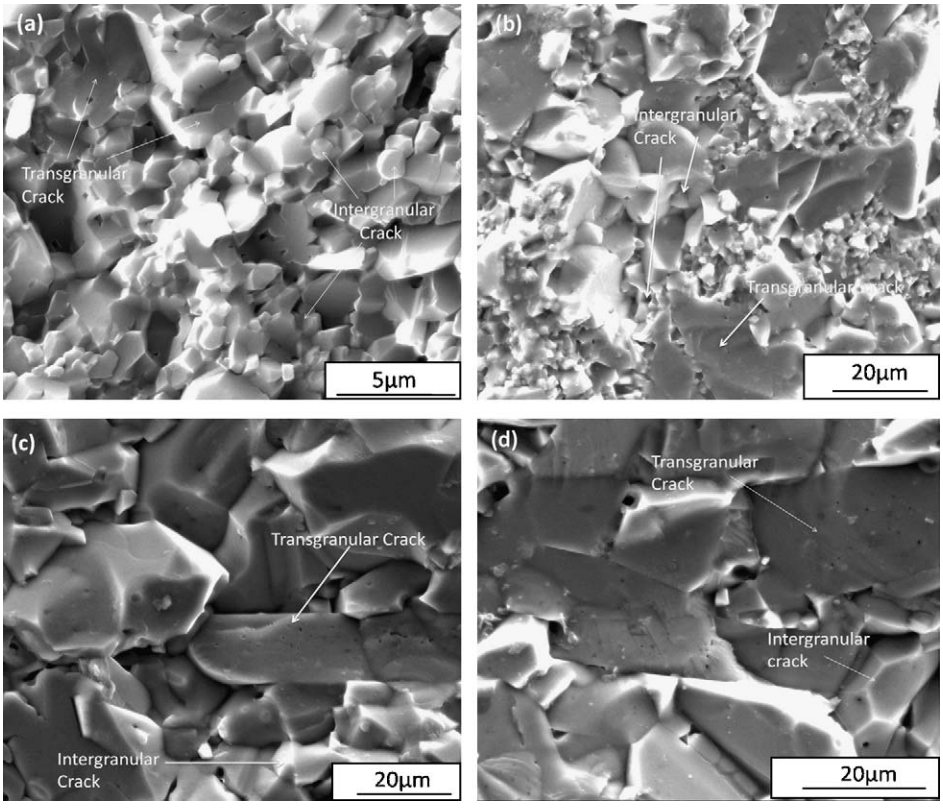

Fig. 7. SEM micrograph of Fracture surface of Al_2O_3 sample sintered at (a) 1500 °C for 3 h, (b) 1500 °C for 18 h, (c) 1600 °C for 3 h and (d) 1700 °C for 3 h.

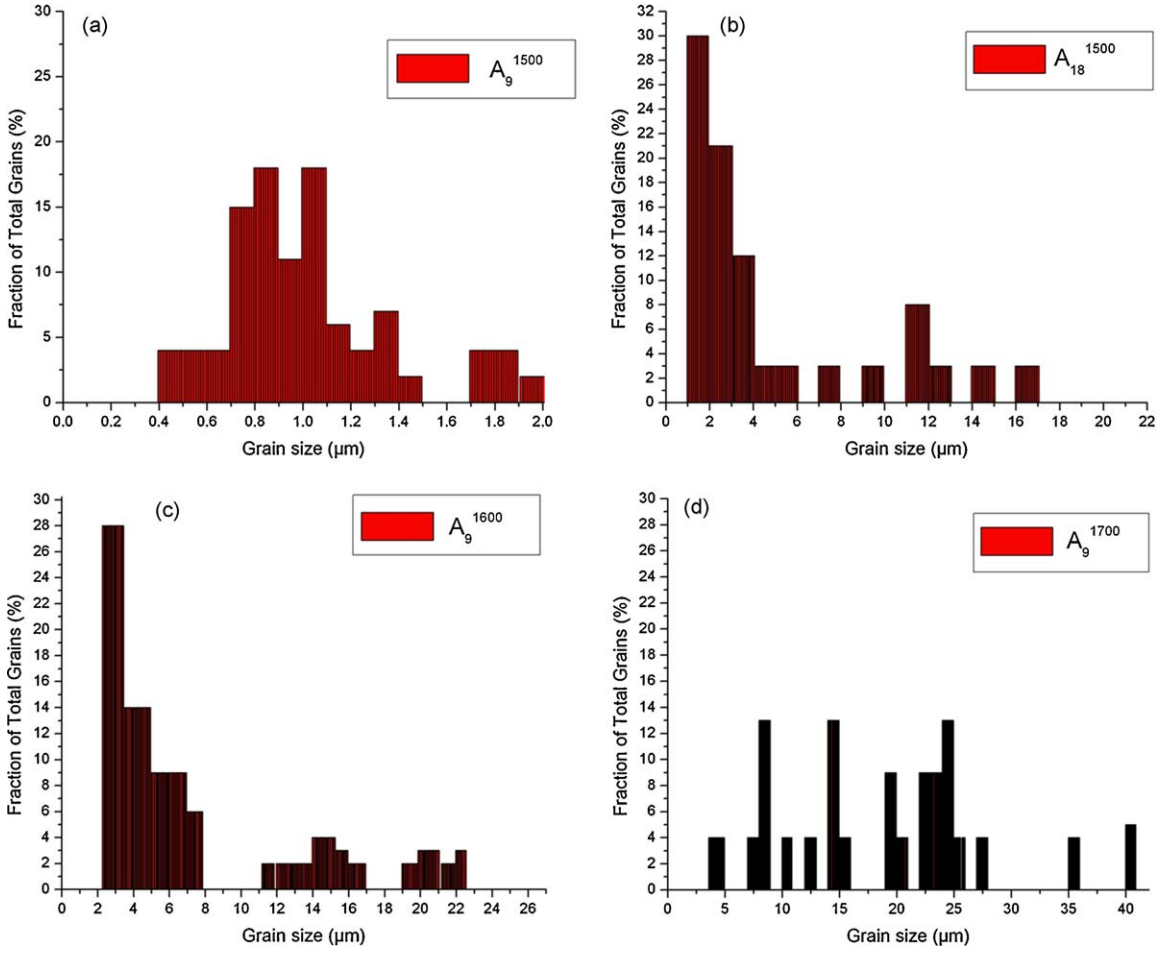

Fig. 8. Grain size histograms for the samples of (a) A_9^{1500}, (b) A_{18}^{1500}, (c) A_9^{1600}, and (d) A_9^{1700}.

This observation is also consistent with the microstructure given in Fig. 2(a). Though the fracture by transgranular type is present, but intergranular fracture mode is clear from Fig. 7(c) and also from Fig. 5(b).

As the grains in all the samples vary over a range of size rather than preferably having uniform size for a particular sintering schedule, it is appropriate to show the actual size distribution that has been resulted. The measured grain sizes were subdivided into small size intervals and plots were made in the form of histograms to show the grain size distribution. Fig. 8 presents a few of such histograms for the samples sintered at 1500, 1600 and 1700 °C. It can be seen from Fig. 8(a) that though the grains in the sample are of different sizes varying from about 0.4 to about 2 μm, a large number of grains fall between 0.7 and 1.1 μm. However, the grains are significantly smaller in this case compared to those in other samples shown in the histogram plots. Similarly Fig. 8(b) and (c) shows that though there is a wide variation in the grain size in the samples, a large number of grains fall in the size range of 1–4 μm according to Fig. 8(b) and in 2–8 μm corresponding to Fig. 8(c). Therefore the grain size distribution in Fig. 8(a)–(c), can approximately be taken as bimodal type. However discontinuities in grain size variation are observed over 6–17 μm in Fig. 8(b) and 8–23 μm in Fig. 8(c). Whereas, no clusters showing relatively uniform grain size as has been found in Fig. 8(a)–(c), can be observed in Fig. 8(d) which implies that the grain size distribution in Fig. 8(d) is rather more wide and the distribution can be treated far from bimodal type. The grain size variation in Fig. 8(d) is discontinuous across the entire grain size range. The main purpose of showing the grain size measurements in the form of histograms in a few cases is to demonstrate the influence of the grain size distribution on fracture toughness behaviour through the proposed mechanisms of grain bridging and crack deflections that become effective with bimodal type grain size distribution [22,23].

Fig. 9 shows data points plotted between fracture toughness and fracture surface roughness of the samples sintered at 1500, 1600 and 1700 °C. A best fit line has been drawn through these data points. It can be seen that data points in the higher range of fracture toughness fall on or very close to the straight line whereas, the points in the lower fracture toughness region are situated far apart from the straight line. This means that the samples with lower fracture toughness do not follow the same linear relationship when extended to the lower fracture toughness region. Boccaccini and Winkler [14] have shown the linear correlation between the fracture toughness and fracture surface roughness which gives rise to the crack

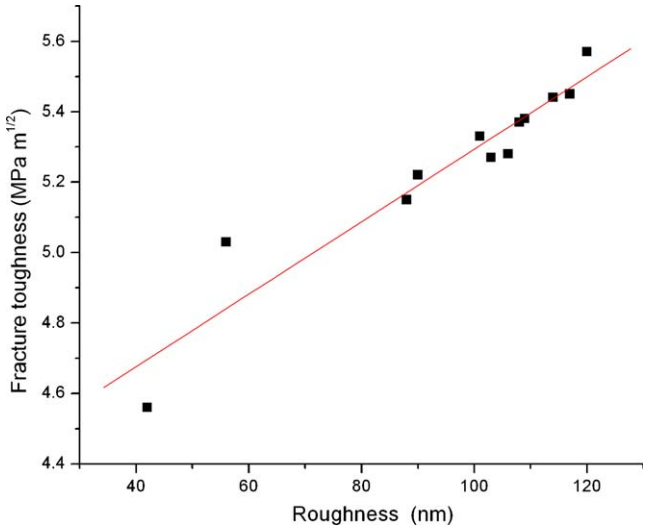

Fig. 9. Fracture toughness vs fracture surface roughness of the samples sintered at 1500, 1600 and 1700 °C.

deflection as the toughening mechanism in the Al_2O_3 platelet reinforced glass matrix composites.

4. Conclusions

The following are the conclusions of the present study:

(1) The Al_2O_3 ceramics prepared by solid state sintering at three different temperatures of 1500, 1600 and 1700 °C for different soaking time periods have the range of grain size variation from as low as 0.2–1.3 μm for the samples sintered at 1500 °C and for 3 h to as high as 4.3–41.2 μm when sintered at 1700 °C for 12 h.

(2) Fracture toughness of the samples sintered at 1500 °C and for soaking time periods of 3, 6, 9, 12, 18, 24 and 36 h lie in the range of 5.2 ± 0.4–5.4 ± 0.5 MPa $m^{1/2}$. Fracture toughness of the samples sintered at 1600 °C is slightly higher and lies between 5.0 ± 0.4 and 5.6 ± 0.5 MPa $m^{1/2}$ and for the samples sintered at 1700 °C the fracture toughness is less than that of the samples sintered at 1500 and 1600 °C and the value lies between 4.6 ± 0.5 and 5.0 ± 0.6 MPa $m^{1/2}$.

(3) Fracture surface study reveals that mixed mode of fracture i.e. intergranular and transgranular types with larger proportion of former type cause fracture in the samples sintered at 1500 and 1600 °C. Such observation leads to conclude that crack deflection is the primary reason for higher fracture toughness in these samples. Although contribution also comes from grain shape variation expressed through the aspect ratio determinations. The number of grains having larger aspect ratio 1.81–2.85 in the samples sintered at 1600 °C is more compared to the samples sintered at 1500 and 1700 °C.

(4) The fracture surface study reveals that the transgranular fracture as a dominant mode of fracture for the samples sintered at 1700 °C.

(5) The linear relationship between the fracture surface roughness and the fracture toughness is followed well for the samples having higher fracture toughness.

References

[1] Z.Y. Deng, Y. Zhou, M.E. Brito, Y. Tanaka, T. Ohji, Effects of rare earth dopants on grain boundary bonding in alumina–silicon carbide composites, J. Eur. Ceram. Soc. 24 (2004) 511–516.
[2] B.K. Jang, M. Enoki, T. Kishi, H.K. Oh, Effect of second phase on mechanical properties and toughening of Al_2O_3 based ceramic composites, Compos. Eng. 5 (1995) 1275–1286.
[3] G.D. West, J.M. Perkins, M.H. Lewis, The effect of rare earth dopants on grain boundary cohesion in alumina, J. Eur. Ceram. Soc. 27 (2007) 1913–1918.
[4] Z. Xihua, L. Changxia, L. Musen, Z. Jianhua, Research on toughening mechanisms of alumina matrix ceramic composite materials improved by rare earth additive, J. Rare Earths 26 (2008) 367–370.
[5] W.B. Chou, W.H. Tuan, Toughening and strengthening of alumina with silver inclusions, J. Eur. Ceram. Soc. 15 (1995) 291–295.
[6] F.C. Zhang, H.H. Luo, T.S. Wang, S.G. Roberts, R.I. Todd, Influence factors on wear resistance of two alumina matrix composites, Wear 265 (2008) 27–33.
[7] D. Kovar, S.J. Bennison, M.J. Readey, Crack stability and strength variability in alumina ceramics with rising toughness-curve behavior, Acta Mater. 48 (2000) 565–578.
[8] Y. Maniette, M. Inagaki, M. Sakai, Fracture toughness and crack bridging of a silicon nitride ceramic, J. Eur. Ceram. Soc. 7 (1991) 255–263.
[9] P.F. Becher, Microstructural design of toughened ceramics, J. Am. Ceram. Soc. 74 (1991) 255–269.
[10] S.Y. Park, Influence of a liquid phase on the microstructure development of Al_2O_3, J. Mater. Sci. Lett. 15 (1996) 878–880.
[11] L. Xu, Z. Xie, L. Gao, X. Wang, F. Lian, T. Liu, W. Li, Synthesis, evaluation and characterization of alumina ceramics with elongated grains, Ceram. Int. 31 (2005) 953–958.
[12] O.L. Ighodaro, O.I. Okoli, Fracture toughness enhancement for alumina systems: a review, Int. J. Appl. Ceram. Technol. 5 (2008) 313–323.
[13] T. Tani, Y. Miyamoto, M. Koizumi, M. Shimada, Grain size dependences of Vickers microhardness and fracture toughness in $A1_2O_3$ and Y_2O_3 ceramics, Ceram. Int. 12 (1986) 33–37.
[14] A.R. Boccaccini, V. Winkler, Fracture surface roughness of Al_2O_3–plateler reinforced glass matrix composites, Composites A 33 (2002) 125–131.
[15] G.R. Anstis, P. Chantikul, B.R. Lawn, D.B. Marshall, A critical evaluation of indentation techniques for measuring fracture toughness: I, direct crack measurements, J. Am. Ceram. Soc. 64 (1981) 533–538.
[16] R.W. Rice, C.C. Wu, F. Borchelt, Hardness-grain size relation in ceramics, J. Am. Ceram. Soc. 77 (10) (1995) 2539–2553.
[17] R. Baddi, J. Crampon, R. Duclos, Temperature and porosity effects on the fracture of fine grain size MgO, J. Mater. Sci. 21 (1986) 1145–1150.
[18] A.G. Evans, D. Gilling, R.W. Davidge, The temperature-dependence of the strength of polycrystalline MgO, J. Mater. Sci. 5 (1970) 187–197.
[19] H.X. Lu, H.W. Sun, G.X. Li, C.P. Chen, D.L. Yang, X. Hu, Microstructure and mechanical properties of Al_2O_3–MgB_2 composites, Ceram. Int. 31 (2005) 105–108.
[20] S.R. Hah, T.E. Fischer, P. Gruffel, C. Carry, Effect of grain boundary dopants and mean grain size on tribomechanical behavior of highly purified α-alumina in the mild wear regime, Wear 181–183 (1995) 165–177.
[21] Z.Y. Deng, Y. Zhou, M.E. Brito, J.F. Yang, T. Ohji, Fracture-mode change in alumina-silicon carbide composites doped with rare-earth impurities, J. Am. Ceram. Soc. 86 (10) (2003) 1789–1792.
[22] S.H. Kim, Y.W. Kim, M. Mitoma, Microstructure and fracture toughness of liquid-phase-sintered β-SiC containing β-SiC whiskers as seeds, J. Mater. Sci. 38 (2003) 1117–1121.
[23] R. Vaβen, J. Förster, D. Stöver, Toughening of SiC ceramics by a bimodal grain size distribution produced by hiping ultrafine and coarse grained SiC powders, Nanostruct. Mater. 6 (1995) 889–892.